Excited State Properties of 3 '-Hydroxyechinenone in Solvents and in the Orange Carotenoid Protein from Synechocystis sp PCC 6803

ARTICLE *in* THE JOURNAL OF PHYSICAL CHEMISTRY B · MAY 2014

Impact Factor: 3.3 · DOI: 10.1021/jp5041794 · Source: PubMed

3 AUTHORS:

Dariusz M Niedzwiedzki
Washington University in St. Louis
77 PUBLICATIONS **1,245** CITATIONS
SEE PROFILE

Haijun Liu
Washington University in St. Louis
26 PUBLICATIONS **280** CITATIONS
SEE PROFILE

Robert E Blankenship
Washington University in St. Louis
338 PUBLICATIONS **14,607** CITATIONS
SEE PROFILE

THE JOURNAL OF PHYSICAL CHEMISTRY B

Article

pubs.acs.org/JPCB

Excited State Properties of 3′-Hydroxyechinenone in Solvents and in the Orange Carotenoid Protein from *Synechocystis* sp. PCC 6803

Dariusz M. Niedzwiedzki,[‡] Haijun Liu,[‡,§] and Robert E. Blankenship*[,†,‡,§]

[†]Department of Chemistry, [‡]Photosynthetic Antenna Research Center (PARC), [§]Department of Biology, Washington University in St. Louis, One Brookings Drive, St. Louis, Missouri 63130, United States

ABSTRACT: The orange carotenoid protein (OCP) is a 35 kDa water-soluble protein involved in a photoprotective mechanism of the photosynthetic apparatus of cyanobacteria. The OCP protein contains a single molecule of the carotenoid 3′-hydroxyechinenone (3′-hECN). We have performed transient absorption studies at 77 K in the visible and near-infrared spectral ranges on 3′-hECN in solvent glass and in both inactive (orange) and active (red) forms of OCP. In the OCP the cryogenic temperature prohibited the protein from spontaneous conversion between activity stages and allowed us to study well-defined spectral forms of the protein. The studies show that each form of the OCP consists of two protein subpopulations having different photophysical properties of the bound 3′-hECN. At 77 K the inactive OCP reveals two lifetimes of the first excited state of 3′-hECN of 5.2 and 11 ps while in the active form of OCP these are 3.2 and 7.1 ps. We have also determined the energy of the first excited singlet state of 3′-hECN in long-lived subpopulations of both OCP forms at 77 K. This is 13,750 cm^{-1} in the inactive OCP and 12,300 cm^{-1} in the active OCP. Shortening of the lifetime and decrease of the energy of the first excited singlet state of 3′-hECN confirm the lengthening of the effective conjugation of the carotenoid upon the inactive-to-active conversion of OCP.

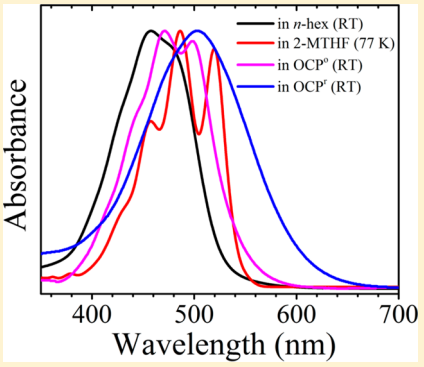

INTRODUCTION

The orange carotenoid protein (OCP) is a 35 kDa water-soluble protein that is involved in a photoprotective mechanism of the photosynthetic apparatus of cyanobacteria.[1−7] The crystal structures of the OCP protein have been determined from two species, *Arthrospira maxima*[8] and *Synechocystis* sp. PCC 6803.[2] The protein contains a single carotenoid molecule, 3′-hydroxyechinenone (3′-hECN) that has 12 conjugated double bonds—11 conjugated C═C bonds extended by a carbonyl group. The crystal structures show that carotenoid significantly changes its geometry upon binding to the protein.[2,8] While in organic solvents, the carotenoid terminal ring that contains the carbonyl group is in an s-cis configuration, in the OCP, the protein−pigment interactions change it to s-trans (Figure 1A). The geometric alteration of the pigment backbone combined together with formation of hydrogen bonds between the carbonyl group of 3′-hECN and tyrosine and tryptophan residues of the OCP-apoprotein influence the S_1 excited state properties of the carotenoid and activates an intramolecular charge transfer state (ICT).[9] Previously it was proposed that upon light-induced activation of the inactive "orange" form (OCP^o) to the active "red" form (OCP^r) by blue-green light, the ICT state of 3′-hECN is formed and lowered until it falls below the singlet excited S_1 of bilin, the pigment molecule in the phycobilisome (PBS). Upon light saturation conditions only the OCP^r form can bind to the PBS and efficiently quench excitation energy transfer from the PBS to the reaction center. However, the exact mechanism of quenching energy or electron transfer between interacting chromophores is still under debate.[10,11] Recent evidence suggests that the inactive orange form of OCP is a dimer and the active red form is a monomer.[12]

The transition between OCP^o and OCP^r forms is fully reversible,[2] and performing spectroscopic studies on both forms of OCP is complicated due to fast activation/deactivation processes that happen within a few seconds at room temperature.[1,2,9,13] Especially in the transient absorption spectroscopy in which intense laser light is applied to promote 3′-hECN into the $S_2(1^1B_u^+)$ excited state, the OCP^o-to-OCP^r transition can be easily triggered at ambient temperatures. In consequence, the spectroscopic results for both spectral forms of the OCP may be actually very similar due to easiness of the OCP^o-to-OCP^r transition process.

Recent spectroscopic investigations performed on the OCP from *Arthrospira maxima* with application of the ultrafast absorption in the NIR range have questioned the importance of proposed alteration of the energy of the first excited singlet state, $S_1(2^1A_g^-)$, of 3′-hECN as a major factor that regulates quenching properties of the active OCP.[9] In order to define the $S_1(2^1A_g^-)$ state energy of 3′-hECN, the authors of that study performed room temperature transient absorption measurements on 3′-hECN in solvents and in the OCP that was presumed to be a mixture of both inactive and active forms. Upon assumption that the $S_1(2^1A_g^-)$ state of 3′-hECN decays with different rates in the OCP^o and OCP^r, the authors used the recorded $S_1(2^1A_g^-) \rightarrow S_2(1^1B_u^+)$ transient bands associated

Received: April 29, 2014
Revised: May 20, 2014
Published: May 20, 2014

   dx.doi.org/10.1021/jp5041794 | *J. Phys. Chem. B* 2014, 118, 6141−6149

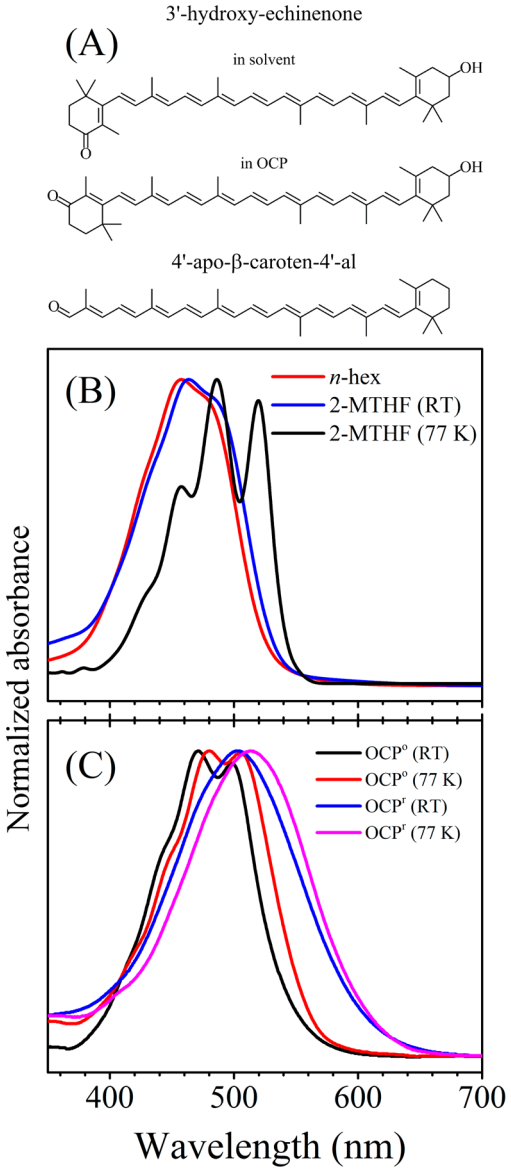

Figure 1. (A) molecular structure of 3′-hECN in solvent and in the OCP crystal structure together with structure of 4′-apo-*β*-caroten-4′-al, (B) steady-state absorption spectra of 3′-hECN in *n*-hex and in 2-MTHF taken at RT and in 2-MTHF at 77 K. The spectra were normalized to their maxima for better comparability. (C) Steady-state absorption spectra of 3′-hECN in the OCP^{o} at RT (black) and at 77 K (red) and in the OCP^{r} at RT (blue) and at 77 K (magenta). The spectra were normalized at their maxima for better comparability.

with those decay constants and obtained the $S_1(2^1A_g^-)$ energy of 3′-hECN in the OCP^{o} and OCP^{r} of 14,650 cm^{-1} and 14,000 cm^{-1}, respectively. It has been demonstrated that indeed, the OCP protein environment alters the $S_1(2^1A_g^-)$ energy of 3′-hECN during photoactivation. If the photophysical properties of OCP-bound carotenoid were the only factors involved in photoprotection, both energies were still low enough to ensure quenching properties of the OCPs.

More recently, another group has done transient absorption studies on both forms of the OCP in the VIS spectral range at cryogenic temperature.[10] Cryogenic temperatures ensure that both samples are homogeneous during measurements (the possibility of spontaneous OCP^{o}-to-OCP^{r} (or *vice versa*) transition is excluded). Interestingly, these studies demonstrated that, regardless of the activation state, the OCP possesses two inherent decay rates of the $S_1(2^1A_g^-)$/ICT state of 3′-hECN and moreover these are practically identical in the both OCP forms (2.0 and 7.5 ps for the OCP^{o} and 2.3 and 7.6 ps for the OCP^{r}). At room temperature, these lifetimes are shorter and match quite well to those that were previously assigned to decay of the $S_1(2^1A_g^-)$ state of 3′-hECN in two distinct OCPs. These findings seriously question the accuracy of the $S_1(2^1A_g^-)$ energy of 3′-hECN state in the OCP^{o} and OCP^{r} and leave this aspect still open for speculations.

Attempts at explanation of the mechanism of the OCP photoactivation were most recently approached from the viewpoint of mass spectrometry. Application of the native mass spectroscopy revealed that photoactivation of the OCP is also associated with monomerization of the protein that in the inactive state is mostly present as a dimer.[12] These findings may suggest that the actual role of light-induced change of the carotenoid geometry is to influence protein ability to form dimers and changes in the photophysical properties of 3′-hECN are simply the side effects associated with OCP monomerization.

The overall goal of this task was to perform the most comprehensive time-resolved absorption studies of 3′-hECN with special focus on attempt of defining the $S_1(2^1A_g^-)$ energy of 3′-hECN in both forms of the OCP protein and compare them with all available peers. We have done studies on the isolated 3′-hECN at room temperature and at 77 K and on the OCP^{o} and OCP^{r} proteins that were locked in their activity states by freezing to 77 K prior to spectroscopic measurements. We have done measurements in the VIS (400−800 nm) and NIR (800−1600 nm) spectral ranges in order to reveal not only dynamic characteristics of the excited states but also determine the energy of the first excited singlet state of 3′-hECN in various environments and temperatures. Finally, we have compared excited state properties of 3′-hECN that were obtained here with available information and have attempted to build a more general view of the photophysical properties of the isolated and OCP-bound 3′-hECN.

MATERIALS AND METHODS

Purification of 3′-hECN and Preparation for Spectroscopic Measurements. The carotenoid 3′-hECN was extracted from the bulk OCP preparation using technical grade methanol. The extract was filtered and injected into an Agilent 1100 HPLC system employing a reverse phase column Zorbax Eclipse XDB-C18 (250 mm × 4.6 mm) and eluted using acetonitrile/tetrahydrofuran (95:5, v/v) as a mobile phase with 1.5 mL min^{-1} flow rate. For low-temperature measurements, the purified pigment was dissolved in spectroscopic grade 2-methyltetrahydrofuran (2-MTHF), transferred to a 1 cm square cryogenic quartz cuvette and frozen in the SVP100 liquid nitrogen cryostat from Janis (Woburn, MA). The optical density of the sample (OD) was set to ∼0.5 at the maximum of absorption band.

Preparation of OCP for Spectroscopic Measurements. The OCP was isolated as described elsewhere.[12] In order to make the buffer transparent in the NIR range, D_2O was used instead of normal water. To obtain the OCP in the OCP^{o} form, the fresh OCP sample was mixed with glycerol at ratio 1:1 (v/v), transferred into a 1 cm square plastic cuvette, placed into the SVP100 liquid nitrogen Janis cryostat chamber, kept in dark for ∼10 min at room temperature (RT) and subsequently slowly frozen (also in dark) to 77 K. To obtain the OCP in the

dx.doi.org/10.1021/jp5041794 | J. Phys. Chem. B 2014, 118, 6141−6149

OCP^r form, the freshly prepared OCP^o sample was placed into liquid nitrogen cryostat chamber set to RT then continuously illuminated for ∼2 min with intense light and subsequently slowly frozen (with light on during freezing process) to 77 K. The steady-state absorption of OCP^r at RT was taken on the OCP that was continuously illuminated for ∼1 min and then immediately recorded by spectrophotometer working in a fast scan mode. For illumination, a tungsten lamp was used. The light was first filtered through a 10-cm layer of water and then a band-pass (300−800 nm) filter. The light intensity on the sample surface was adjusted to ∼2500 $\mu m \cdot m^{-2} \cdot s^{-1}$. The optical density of the sample (OD) was set to ∼0.5 at the maximum of the absorption band. All steady-state absorption measurements were done using a Shimadzu UV-1800 spectrophotometer. The steady-state and time-resolved absorptions at 77 K were done immediately following each other on the same samples. Integrity of the samples during time-resolved measurements was controlled by taking steady-state absorption after the measurements. No changes in the spectra had been observed.

Femtosecond Time-Resolved Absorption Spectroscopy. Time-resolved pump−probe absorption experiments were carried out using Helios, a femtosecond transient absorption (TA) spectrometer (UltrafastSystems LCC, Sarasota, FL) coupled to a Spectra-Physics femtosecond laser system described previously in detail.[14] The excitation wavelengths for 3′-hECN were chosen as follow: 485 nm in *n*-hexane (*n*-hex), 520 nm in 2-MTHF at 77 K, 505 nm in the OCP^o at 77 K, and 540 nm in the OCP^r at 77 K. The energy of the pump beam was 500 nJ in a spot size of 1 mm diameter corresponding to an intensity of ∼2×10^{14} photons/cm^2.

RESULTS

Room Temperature and 77 K Steady-State Absorption Spectroscopy of 3′-hECN in Solution and in the OCP. The carotenoid 3′-hECN has 11 conjugated C=C bonds (N = 11), terminated by a carbonyl group (C=O) (Figure 1A). These two features determine the appearance of the $S_0(1^1A_g^-) \rightarrow S_2(1^1B_u^+)$ electronic absorption which in low dielectric solvents peaks at ∼460 nm (band center) and is responsible for the yellow color of the pigment. The electronic transition between the $S_0(1^1A_g^-)$ and $S_1(2^1A_g^-)$ states is forbidden owing to selection rules (see refs 15,16 for review). In solution, 3′-hECN adopts the structural geometry as shown in Figure 1A. Room temperature and 77 K absorption spectra of 3′-hECN taken in *n*-hex and 2-MTHF show that lowering of temperature causes a substantial spectral shift of the electronic absorption band toward longer wavelengths. The spectral shift is associated with an increase of polarizability of the molecular environment (Figure 1B). The (0−0) vibronic band of the $S_0(1^1A_g^-) \rightarrow S_2(1^1B_u^+)$ electronic absorption, which is barely resolved at RT and 480 nm (20,800 cm^{-1}) shifts to 520 nm (19,230 cm^{-1}) at 77 K.

The cryogenic temperature substantially enhances resolution of the vibronic structure of the $S_0(1^1A_g^-) \rightarrow S_2(1^1B_u^+)$ transition. Although the nominal conjugation of this carotenoid in solution is assumed to be N = 11+C=O, effectively it is shorter. Based on the recent comprehensive studies of the relationship between the energy of the (0−0) vibronic band of the $S_0(1^1A_g^-) \rightarrow S_2(1^1B_u^+)$ electronic transition and the length of conjugation (N) done on a series of open chain carotenoids with intact C=C conjugation, one can calculate that the effective conjugation (N_{ef}) of 3′-hECN is ∼9.8 double bonds, not nominal 12 (11+C=O).[17] This is simple because double bonds from terminal rings of the carotenoid do not equally contribute to the conjugation as those from molecule's backbone.

Upon binding to the inactive OCP^o (RT) (Figure 1C), the (0−0) vibronic band of the electronic absorption of 3′-hECN shifts from 480 to 498 nm (20,080 cm^{-1}) and is accompanied by a partial recovery of the vibronic resolution. The spectral shift of a carotenoid absorption spectrum in a protein is caused mainly by the large polarizability of protein binding pocket. A typical energy downshift of carotenoid electronic absorption, observed in other pigment−protein complexes like LH2 or LH1 - light-harvesting proteins from purple photosynthetic bacteria, is between 900 and 1,200 cm^{-1}.[18] Upon the assumption the OCP apoprotein interacts similarly with the carotenoid pigment and the carotenoid is bound into the OCP^o with preserved solvent geometry, the (0−0) vibronic band of the $S_0(1^1A_g^-) \rightarrow S_2(1^1B_u^+)$ absorption spectrum of OCP-bound 3′-hECN should lie between 502 and 510 nm (19,920 and 19,600 cm^{-1}).

As discussed above, the (0−0) vibronic band of the $S_0(1^1A_g^-) \rightarrow S_2(1^1B_u^+)$ transition of 3′-hECN in the OCP^o appears at 498 nm at RT. It suggests that N_{ef} of the OCP^o-bound 3′-hECN may be even shorter than one observed in solution and falls in 9.0−9.6 range.

Interestingly, the spectral shape of the OCP^o absorption spectrum (RT) from our studies is different from its counterparts available from work done by other groups. In our sample, the ratio of the (0−0) to the (0−1) vibronic band is ∼0.96, while in all absorption spectra available in literature it is typically >1.[1−3,6,7,13] It demonstrates that the OCP protein with an absorption spectrum of carotenoid that resembles a conventional pattern of an electronic absorption, (0−1) vibronic band being always larger than (0−0), may be actually prepared; however, it requires continuous dark conditions during purification, storage, and measurements. We have observed that, if OCP^o-to-OCP^r conversion is initiated, the OCP does not convert back completely to the initial spectral form of the OCP^o (Figure 1C, black line), and the absorption spectrum will resample the spectral shape known from the literature sources. It points out, that the majority of the OCP^o proteins previously studied were already contaminated by the OCP^r form. Contamination can occur very easily because of spontaneous OCP^o-to-OCP^r transition that happens even at low light. Thus, we think that the OCP^o studied here is probably the best example of pure OCP^o form that has been investigated using time-resolved absorption spectroscopy.

Lowering the temperature to 77 K shifts the absorption spectrum of the OCP^o to longer wavelengths by ∼7 nm to 505 nm (19,800 cm^{-1}) and causes also some loss in vibronic resolution. Loss of vibronic resolution in the absorption spectrum appears to be abnormal. Typically, cryogenic temperature significantly improves spectral resolution. We hypothesize that low temperature affects the geometry of the OCP-bound carotenoid in a way similar to light activation (although not so dramatic), but a definitive conclusion cannot be provided without supplementary studies.

The absorption spectra of the OCP^r taken at RT and at 77 K are given in Figure 1C. The absorption spectrum appears as a featureless band with maximum at 503 nm (19,880 cm^{-1}) at RT and at 514 nm (19,450 cm^{-1}) at 77 K. The 77 K steady-state absorption spectrum of the OCP^r is substantially different from the only one available in the literature, in which the band maximum is centered at 506 nm.[10] Substantial band-shift of

dx.doi.org/10.1021/jp5041794 | J. Phys. Chem. B 2014, 118, 6141−6149

absorption spectrum of 3′-hECN toward longer wavelengths upon the OCP°-to-OCP^r conversion (at RT the center of the absorption band shifts from ∼477 to 503 nm) is associated with a substantial elongation of the effective carotenoid conjugation.[11] Based on the similar rationale as was given earlier in the text, N_{ef} of 3′-hECN in the OCP^r may be expected to fall in the 11−12 range.

Remarkably, 3′-hECN in the geometry as shown in the OCP crystal structure should be spectroscopically very similar to the synthetic apo-carotenal, 4′-apo-β-caroten-4′-al. Its chemical structure is also given in Figure 1A. Because spectroscopic properties of 4′-apo-β-caroten-4′-al such as steady-state absorption and first excited state lifetime had been studied in few solvents, some comparative analysis can be done.[19] The steady-state absorption of 4′-apo-β-caroten-4′-al in low dielectric solvents (*n*-hex, methanol) has a broad shape with maximum (band center) at 483 nm. If it is assumed that binding of this pigment into the protein environment shifts its electronic absorption spectrum by 900−1200 cm^{-1} to lower energies, the maximum of the shifted absorption band will appear between 505 and 513 nm very close to in the range in which the center of absorption of OCP^r-bound 3′-hECN appears.

Femtosecond Time-Resolved Absorption Spectroscopy of 3′-hECN in Organic Solvents at RT and at 77 K. Transient absorption results of 3′-hECN obtained in *n*-hex at RT are given in Figure 2. Figure 2A shows the 2D-profile of TA taken in the VIS spectral range. The bands visible in the contour are labeled and correspond either to bleaching of the ground state absorption (GSA, negative) or excited state absorption (ESA, positive). To get further insights into the dynamics of the excited states, the TA data set was globally analyzed with application of the model that assumes sequential decay of the excitation.[20] The results of the fitting (EADS) are given in Figure 2B. Fitting has revealed three kinetic components with lifetimes of 0.16, 0.65, and 5.8 ps. The uncertainties of fitting did not exceed 5% (here and so on) and are omitted for clarity. The first EADS is associated with decay of the $S_2(1^1B_u^+)$ state and exhibits combined bleaching of the $S_0(1^1A_g^-) \rightarrow S_2(1^1B_u^+)$ transition and stimulated $S_2(1^1B_u^+) \rightarrow S_0(1^1A_g^-)$ emission. The next two EADS are associated with the $S_1(2^1A_g^-)$ state and have lifetimes corresponding to vibrational relaxation (0.65 ps) and state decay (5.8 ps). The quality of fit can be evaluated in Figure 2C, which shows a representative kinetic trace taken at the maximum of the ESA band ($S_1(2^1A_g^-) \rightarrow S_n$) with the corresponding fit. Figure 2D shows the 2D-profile of TA taken in the NIR spectral range. Based on the fitting results it can be concluded that it contains two distinct ESA bands corresponding to the $S_2(1^1B_u^+) \rightarrow S_n$ (a sharp band with maximum ∼1100 nm, 0.16 ps lifetime) transition and a weaker band with longer decay constant of 5.5 ps, associated with the $S_1(2^1A_g^-) \rightarrow S_2(1^1B_u^+)$ ESA. The representative kinetic traces are given in Figure 2F. The amplitude of the trace from 1490 nm was adjusted for better comparability and clarity of figure.

Analogous data sets and analysis of the TA of 3′-hECN in 2-MTHF at 77 K are shown in Figure 3.

Cryogenic temperature has multiple effects on temporal and spectroscopic properties of the excited states. Substantial influence is observed on the lifetime of the $S_1(2^1A_g^-)$ state that elongates to 11.0 ps (Figure 3B). The ESA bands, similarly to GSA, show improved vibronic resolution. The main ESA band in the VIS range is shifted to longer wavelengths with

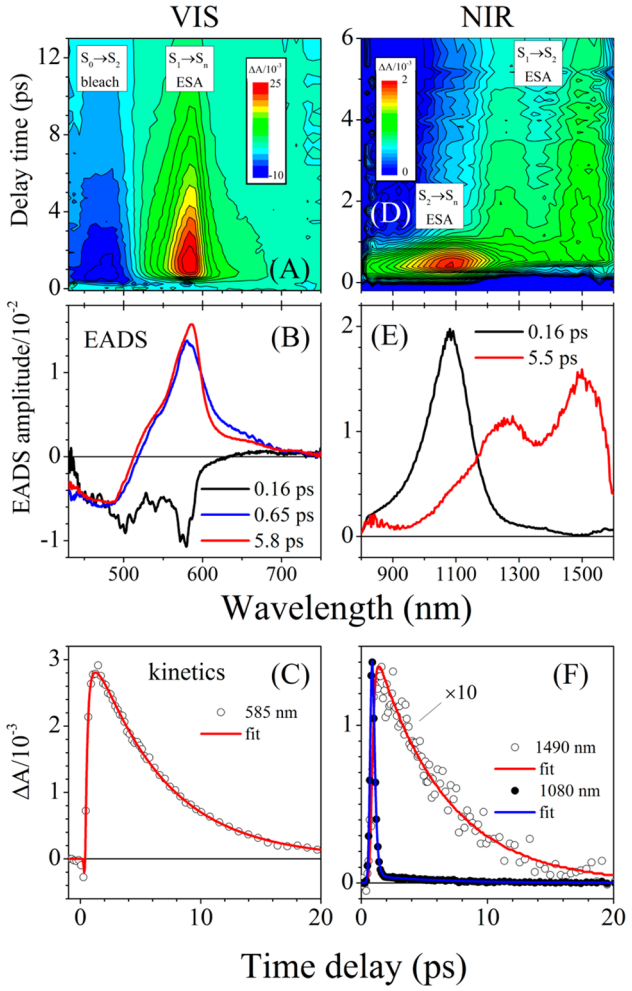

Figure 2. Spectral and temporal properties of the excited states of 3′-hECN in *n*-hex, (A) Color-coded, two-dimensional contour of TA of 3′-hECN taken in the VIS range upon excitation at 485 nm. (B) Results of global analysis of the VIS TA data set, (C) Representative dynamics of decay of the $S_1(2^1A_g^-)$ state probed at maximum of the $S_1(2^1A_g^-) \rightarrow S_n$ ESA band accompanied by fit obtained from global analysis. (D) Color-coded, two-dimensional contour of TA of 3′-hECN taken in the NIR range upon excitation at 485 nm. (E) Results of global analysis of the NIR TA data set. (F) Representative dynamics of decay of the $S_2(1^1B_u^+)$ and $S_1(2^1A_g^-)$ states probed at the $S_2(1^1B_u^+) \rightarrow S_n$ (blue) and the $S_1(2^1A_g^-) \rightarrow S_2(1^1B_u^+)$ (red) ESA bands, accompanied by fits obtained from global analysis.

respect to RT and has a maximum appearing at ∼620 nm (16,100 cm^{-1}) (∼580 nm at RT) (Figure 3B). Due to the fact that a large polarizability of the 2-MTHF glass shifts the steady-state absorption spectrum toward longer wavelengths, the energetic gap between the $S_1(2^1A_g^-)$ and $S_2(1^1B_u^+)$ states narrows. That is visible as spectral shift of the $S_1(2^1A_g^-) \rightarrow S_2(1^1B_u^+)$ transition toward longer wavelengths (Figure 3E). The quality of fitting is shown in Figure3C,F with the representative kinetic traces extracted from the VIS and NIR data sets and associated fits.

Knowledge of both the $S_0(1^1A_g^-) \rightarrow S_2(1^1B_u^+)$ steady-state and the $S_1(2^1A_g^-) \rightarrow S_2(1^1B_u^+)$ time-resolved absorption allows us to calculate the energy of the optically forbidden $S_1(2^1A_g^-)$ state. It is demonstrated in Figure 4.

Both spectral profiles were first converted to a wavenumber scale, and then the $S_1(2^1A_g^-) \rightarrow S_2(1^1B_u^+)$ ESA was shifted until it gave the best coincidence with the steady-state

dx.doi.org/10.1021/jp5041794 | J. Phys. Chem. B 2014, 118, 6141−6149

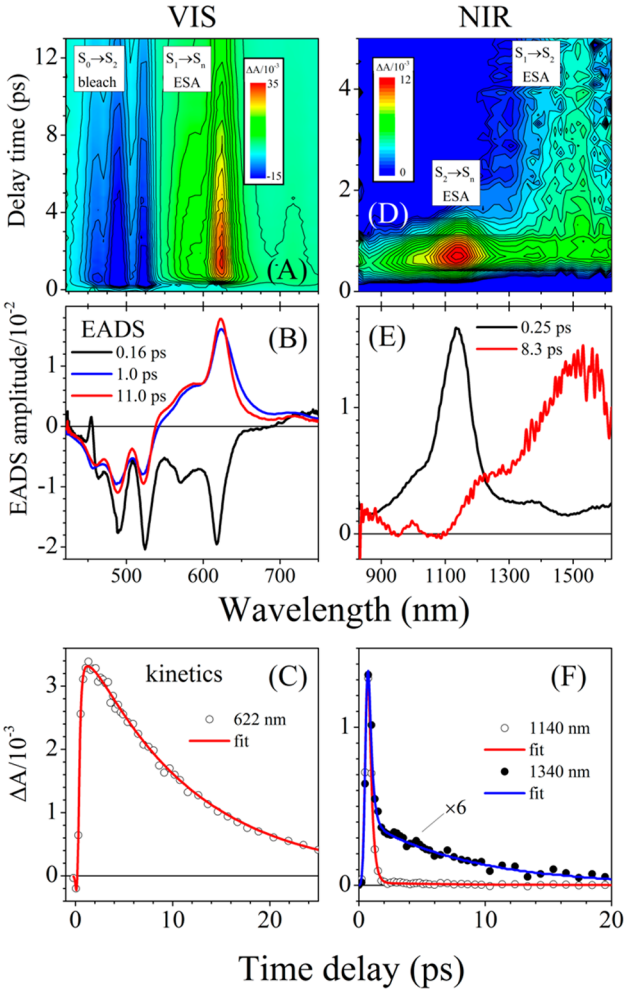

Figure 3. Spectral and temporal properties of the excited states of 3′-hECN in 2-MTHF at 77 K. (A) Color-coded, two-dimensional contour of TA of 3′-hECN taken in the VIS range upon excitation at 520 nm. (B) Results of global analysis of the VIS TA data set. (C) Representative dynamics of decay of the $S_1(2^1A_g^-)$ state probed at maximum of the $S_1(2^1A_g^-) \rightarrow S_n$ ESA band, accompanied by fit obtained from global analysis. (D) Color-coded, two-dimensional contour of TA of 3′-hECN taken in the NIR range upon excitation at 520 nm. (E) Results of global analysis of the NIR TA data set. (F) Representative dynamics of decay of the $S_2(1^1B_u^+)$ and $S_1(2^1A_g^-)$ states probed at the $S_2(1^1B_u^+) \rightarrow S_n$ (blue) and the $S_1(2^1A_g^-) \rightarrow S_2(1^1B_u^+)$ (red) ESA bands, accompanied by fits obtained from global analysis.

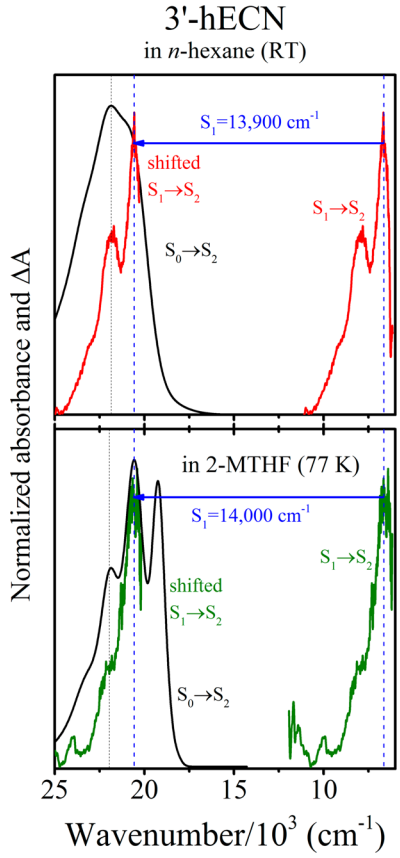

Figure 4. Determination of the $S_1(2^1A_g^-)$ state energy by comparison of the $S_1(2^1A_g^-) \rightarrow S_2(1^1B_u^+)$ ESA with the steady-state $S_0(1^1A_g^-) \rightarrow S_2(1^1B_u^+)$ absorption. The spectra are plotted on wavenumber scale. The shift required to bring both spectra to the best coincidence determines the $S_1(2^1A_g^-)$ state energy. As seen, the energy is not substantially influenced by temperature.

absorption spectrum. The shift determines that $S_1(2^1A_g^-)$ energy is 13,900 ± 50 cm^{-1} in *n*-hex at RT and 14,000 ± 50 cm^{-1} in 2-MTHF at 77 K and shows that it is not influenced by temperature.

Femtosecond Time-Resolved Absorption Spectroscopy of 3′-hECN in OCP at 77 K. The 77 K transient absorption data and global analysis results of the OCP° excited at 505 nm are shown in Figure 5.

In the VIS range the TA spectra show features similar to those observed for 3′-hECN in organic solvents; however, few differences are clearly visible. The ESA band is significantly broader with the maximum appearing at ∼670 nm. Global analysis revealed three kinetic components, first with lifetime associated with decay of the $S_2(1^1B_u^+)$ but shorter than the width of the instrument response function (IRF, fwhm ≈ 150 fs) and two longer-living components with lifetimes of 5.2 and 11 ps. The latter two EADS have vastly different spectral shapes and amplitudes suggesting that the OCP° is not intrinsically homogeneous and contains subpopulations binding 3′-hECN in two different geometries with vastly diverse temporal and spectroscopic properties of the lowest excited state. Three representative kinetic traces extracted at 514 nm (bleaching of the ground state absorption), 570 nm (range that has largest contribution to the 11 ps decay component), and 668 nm (maximum of the ESA band) are given in Figure 5C. Upon shifting of the probe range into the NIR (Figure 5D), the TA data reveal also three kinetic components with lifetimes, as observed in the VIS range (Figures 5B and E). The second and third EADS component are multiplied 20 times in order to make them comparable to the overwhelming $S_2(1^1B_u^+) \rightarrow S_n$ band visible in the first EADS. As seen, the second EADS that contains clearly resolved peak at 1350 nm associated with one of the vibronic bands of the $S_1(2^1A_g^-) \rightarrow S_2(1^1B_u^+)$ transition also shows a small negative dip between 1100 and 1250 nm. Numerous investigations on carbonyl-containing carotenoids demonstrated that such a spectral feature is associated with stimulated emission (SE) from an ICT state that is induced upon an increase of polarity of the carbonyl carotenoid environment.[19,21−31] Presence of this feature suggests that some portion of the OCP° contains 3′-hECN with the $S_1(2^1A_g^-)$ state that already retains some ICT character. The last EADS does not show this spectral feature and resembles the classical shape of the $S_1(2^1A_g^-) \rightarrow S_2(1^1B_u^+)$ transition.

dx.doi.org/10.1021/jp5041794 | J. Phys. Chem. B 2014, 118, 6141−6149

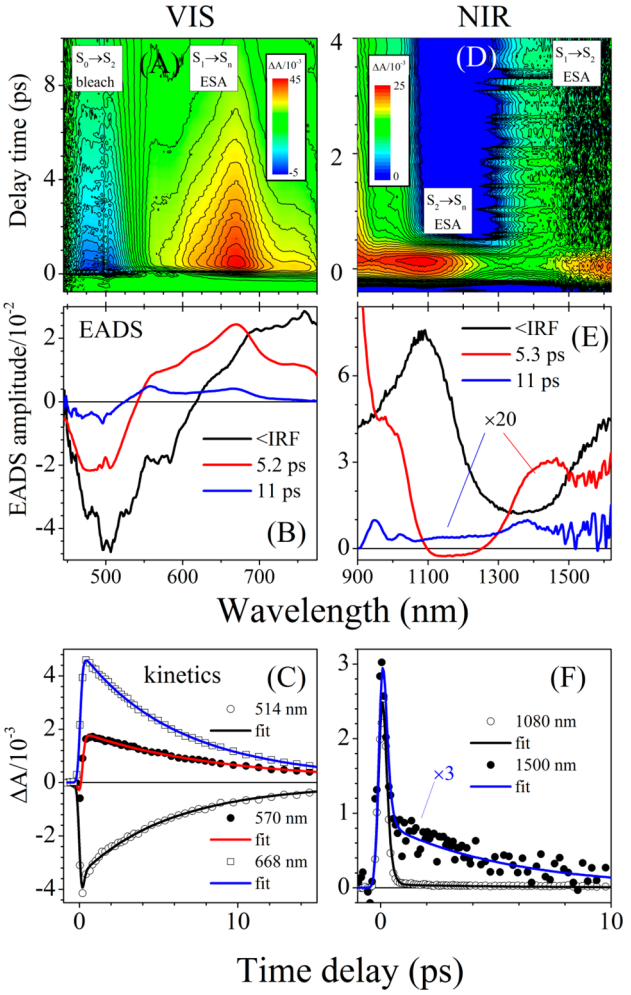

Figure 5. Spectral and temporal properties of the excited states of 3′-hECN in OCP^o at 77 K, (A) Color-coded, two-dimensional contour of TA of OCP^o taken in the VIS range upon excitation at 505 nm. (B) Results of global analysis of the VIS TA data set. (C) Representative dynamics of decay of the $S_1(2^1A_g^-)$ state probed at various points of the broad ESA band accompanied by fits obtained from global analysis. (D) Color-coded, two-dimensional contour of TA taken in the NIR range upon excitation at 505 nm. (E) Results of global analysis of the NIR TA data set. (F) Representative dynamics of decay of the $S_2(1^1B_u^+)$ and $S_1(2^1A_g^-)$ states probed at the maximum of the $S_2(1^1B_u^+) \rightarrow S_n$ ESA band (black) and at long wavelength edge of the $S_1(2^1A_g^-) \rightarrow S_2(1^1B_u^+)$ (blue) ESA, accompanied by fits obtained from global analysis.

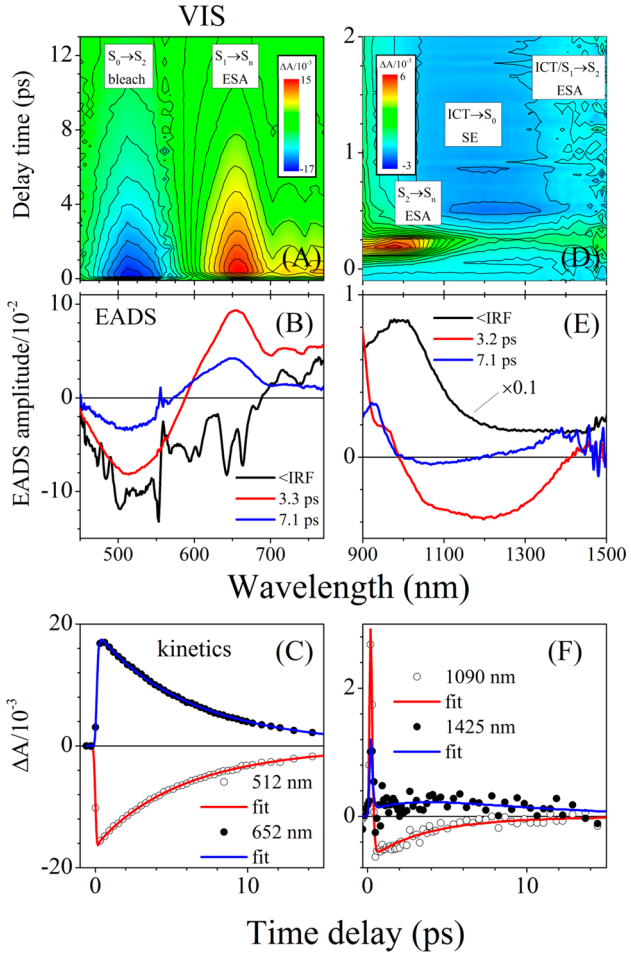

Figure 6. Spectral and temporal properties of the excited states of 3′-hECN in OCP^r at 77 K (A) Color-coded, two-dimensional contour of TA of OCP^r taken in the VIS range upon excitation at 540 nm. (B) Results of global analysis of the VIS TA data set. (C) Representative dynamics of decay of the ICT/$S_1(2^1A_g^-)$ state probed at the ESA band and at the ground state absorption bleaching, accompanied by fits obtained from global analysis. (D) Color-coded, two-dimensional contour of TA of OCP^r taken in the NIR range upon excitation at 540 nm. (E) Results of global analysis of the NIR TA data set. (F) Representative dynamics of decay of the $S_2(1^1B_u^+)$ and ICT states. SE = stimulated emission.

Figure 5F shows two illustrative kinetics taken at the maximum of the $S_2(1^1B_u^+) \rightarrow S_n$ band (1080 nm) and at the range in which the $S_1(2^1A_g^-) \rightarrow S_2(1^1B_u^+)$ transition mostly contributes (1500 nm).

Figure 6 shows 77 K TA data and global analysis results of the OCP^r excited at 540 nm. Global analysis of the VIS data set (Figure 6A) revealed three kinetic components (Figure 6B). The first EADS with lifetime shorter than width of the IRF function is associated with decay of the $S_2(1^1B_u^+)$ state (Figure 6B). Unfortunately, this EADS is considerably obscured with a strong response from the frozen buffer. The second and third EADS with lifetimes of 3.3 and 7.1 ps demonstrate similar spectral shapes with the characteristic broad ESA band peaking at ~655 nm; however, both components have vastly different amplitudes. TA taken in the NIR spectral range reveals a spectral feature that was barely visible in the OCP^o—a noticeable SE band, ranging between 1000 and 1450 nm and present within a few picoseconds after initial excitation. Global analysis of the NIR data set (Figure 6E) shows that the SE is mainly associated with 3.2 ps EADS, one that has the highest amplitude in the VIS spectral range. The line shape of the 7.1 ps EADS in the NIR is somewhat similar to 5.3 ps EADS from the OCP^o, which also contains a partially resolved $S_1(2^1A_g^-) \rightarrow S_2(1^1B_u^+)$ transition with the vibronic band at ~1380 nm distorted by a trace of SE at shorter wavelengths. The characteristic dynamics of the excited states recorded in the VIS and NIR ranges, supplemented with fits are given in Figure 6C,F.

Figure 7 shows the estimation of the $S_1(2^1A_g^-)$ energy of the OCP^o-bound 3′-hECN using the same procedure that was applied for 3′-hECN in solvents. Analysis of the steady-state absorption of the OCP^o (earlier in the text) proposes that the effective length of the double bond conjugation of 3′-hECN remains more or less the same in the OCP^o as in solvent and rather a minor variation of the $S_1(2^1A_g^-)$ energy is expected.

dx.doi.org/10.1021/jp5041794 | J. Phys. Chem. B 2014, 118, 6141−6149

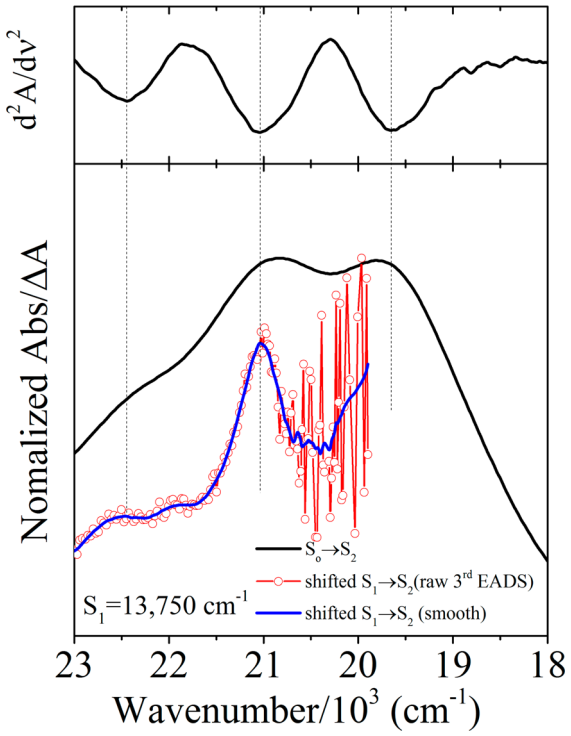

Figure 7. Determination of the $S_1(2^1A_g^-)$/ICT state energy of 3′-hECN in the OCP^o subpopulation with longer excited state lifetime, done by comparison of the $S_1(2^1A_g^-)$/ICT → $S_2(1^1B_u^+)$ ESA with the steady-state $S_0(1^1A_g^-)$ → $S_2(1^1B_u^+)$ absorption. The spectra are plotted on wavenumber scale. The shift required to bring both spectra to the best coincidence determines the $S_1(2^1A_g^-)$ state energy. For better visualization of positions of the vibronic bands of the steady-state absorption the second derivative of the spectrum is also shown. The minima in the second derivative profile correspond to the positions of vibronic bands.

Upon such an assumption, the best coincidence in overlay of both the steady-state absorption and the $S_1(2^1A_g^-)$ → $S_2(1^1B_u^+)$ ESA profile taken from the third EADS is obtained if the state energy is set to 13,750 ± 100 cm^{-1}. Alignment of both spectral profiles was supported by the second derivative of the steady-state absorption that more adequately shows the positions of the vibronic bands. Shifting the $S_1(2^1A_g^-)$ → $S_2(1^1B_u^+)$ ESA to a different vibronic band of the steady-state absorption will give rather unacceptable range of the $S_1(2^1A_g^-)$ energy—above 15,000 or below 12,500 cm^{-1}. It would require 3′-hECN to have a different length of the double bond conjugation and in consequence appearance of the steady-state absorption of the OCP^o at vastly different wavelengths. Estimating the $S_1(2^1A_g^-)$ of 3′-hECN in the major subpopulation of the OCP^o is more difficult due to the fact that (as seen in the second EADS) the $S_1(2^1A_g^-)$ → $S_2(1^1B_u^+)$ line shape is distorted by SE, though a rough assumption can be made based on the relative positions of both EADS would place it ∼300 cm^{-1} below (13,450 cm^{-1}).

Similar analysis for the OCP^r is difficult. The NIR TA data show that first excited state has strong ICT character, and the $S_1(2^1A_g^-)$/ICT → $S_2(1^1B_u^+)$ transient band appearing in the NIR range substantially overlaps with the SE, and the resulting spectrum (combination of both) is practically unusable for any calculation (see second EADS in the global analysis results in Figure 6E). However, the last EADS, presumably associated with the pool of OCP^r containing 3′-hECN with weaker ICT character of the $S_1(2^1A_g^-)$/ICT state, shows the line shape that resolves the vibronic band similar to the one recorded for the OCP^o. Using the methodology as above, with the assumption that the vibronic band of the $S_1(2^1A_g^-)$/ICT → $S_2(1^1B_u^+)$ spectral profile at 1380 nm is associated with transition to the first vibronic level of the $S_2(1^1B_u^+)$ state (as it was assumed for OCP^o), one can calculate the $S_1(2^1A_g^-)$/ICT state of 3′-hECN being ∼12,300 cm^{-1}. It should be noted that in addition it was also assumed that the transition to the first vibronic level of the $S_2(1^1B_u^+)$ from the ground state most likely corresponds to the center of the steady-state absorption at 512 nm (Figure 1C, magenta). The energy of the $S_1(2^1A_g^-)$/ICT state with enhanced ICT character (short-living subpopulation) is impossible to determine due to the overwhelming SE band that overlaps with the $S_1(2^1A_g^-)$/ICT → $S_2(1^1B_u^+)$ transition; however, presumably it is expected to be much lower.

The temporal and spectral characteristics of the excited states of 3′-hECN obtained in this work along with available data from other studies are listed in Table 1.

DISCUSSION

Origin of Two Decay Rates of the S_1 Excited State of 3′-hECN in Inactive and Active OCP. Regardless of the temperature or activation stage (inactive, active) of the OCP, 3′-hECN bound into the protein always demonstrates a biexponential decay of the $S_1(2^1A_g^-)$/ICT state (see Table 1). The early transient absorption studies performed at RT on the OCP suggested that such carotenoid behavior originates from a heterogeneity of the OCP sample that contains at least two OCP subpopulations.[11] Later on, the same authors suggested that the presence of two decay rates is associated with the coexistence of two forms of the OCP, based on RT transient absorption studies performed in the NIR range on the OCP that was presumably a mixture of both OCP^o and OCP^r. The authors claimed that the "red" active OCP was related to the fraction of the OCP decaying with a shorter $S_1(2^1A_g^-)$/ICT lifetime (0.9 ps) while the inactive "orange" form was related to the longer one (3.3 ps). With such a hypothesis, the authors were also able to estimate the energy of the $S_1(2^1A_g^-)$/ICT state of 3′-hECN in both OCPs.[9]

However, the most recent transient absorption studies performed in the VIS range on the OCP^o and OCP^r locked in their activation stages via freezing to 77 K clearly demonstrated that both OCP forms show two intrinsic decay rates of the $S_1(2^1A_g^-)$/ICT state of 3′-hECN. Moreover, the decay lifetimes seem to be almost identical in both OCPs (2.0 and 7.5 ps in OCP^o and 2.3 and 7.6 ps in OCP^r).[10] The authors concluded that it is possible that two decay rates originate from the presence of two subpopulations within the same class of the OCP. The carotenoid would demonstrate the same steady-state absorption properties in both subpopulations. However, the $S_1(2^1A_g^-)$/ICT state properties are more sensitive for environmental changes and will slightly differentiate, leading to different decay times and ESA lineshapes.[10]

The results of our studies even more clearly demonstrate that each OCP class undeniably contains two protein subpopulations. Moreover, since steady-state absorption spectra showed that the samples used here have exceptional spectroscopic purity (contamination from another spectral form of the OCP was practically completely eliminated), the TA results clearly show differences not only in the ESA lineshapes but also in the excited state lifetimes of both OCPs. Such differences were not picked up previously at 77 K.[10] The results of global analysis of

dx.doi.org/10.1021/jp5041794 | J. Phys. Chem. B 2014, 118, 6141−6149

Table 1. Excited States Properties of 3′-hECN in Solvents and in the OCP

solvent or source	Abs_{max} (nm)	Exc. (nm)	ESA_{max} (nm)	τ_1 (ps)	τ_2 (ps)	τ_3 (ps)	S_1 (cm^{-1})	T	ref
				3′-hECN					
n-hex	457, 477	480	585	0.16 (0.16)[a]	0.65	5.8 (5.5)	13 900	RT	this study
2-MTHF	463, 487							RT	this study
2-MTHF	519, 486, 456	520		0.16 (0.25)	1.0	11.0 (8.3)	14 000	77 K	this study
n-hex	476	485	~570	0.23		6.4		RT	11
methanol	476	485	~570	0.185		6.2		RT	11
CS_2	512	520	~625	0.135		6.8		RT	11
n-hex	490					(6.2)	14 300	RT	9
methanol	490					(6.2)	14 300	RT	9
				OCP^o					
(1)	471, 498	n.p.						RT	this study
(1)	479, 505	505	670, 556	<IRF (<IRF)	5.2 (5.4)	11.0 (n.e.)	13 750	77 K	this study
(1)	473, 496	495	~570, ~675	0.34	2	7.5		77 K	10
(1)	473, 496	495	~650	0.06	0.8	4.3		RT	10
(2)	495	495		<0.1		3.3	14 650	RT	9
(1)		475	~650	0.1	1	4.5		RT	1
(2)	496	495	650	<0.1	0.9	3.3		RT	11
(1)	496	495	~640	0.06	0.9	3.8		RT	13
				OCP^r					
(1)	503	n.p.						RT	this study
(1)	513	520	653	<IRF (<IRF)	3.3 (3.2)	7.1 (7.1)	12 300	77 K	this study
(1)	506	550	~660	0.26	2.3	7.6		77 K	10
(1)	n.g.	550		0.06	0.9	3.3		RT	10
(2)	510	495		(<0.1)	(0.9)		14 000	RT	9
(1)	~510	550	~625	0.06	0.6	3.2		RT	13

(1) *Synechocystis* PCC 6803, (2) *Arthrospira maxima*. [a]Lifetimes in parentheses are obtained in NIR spectral range, ESA_{max} - maxima in excited state absorption, RT - room temperature, IRF - width of instrument response function, Abs_{max} - maxima in steady-state absorption, Exc. - excitation wavelength.

the VIS and NIR TA show that inherent lifetimes of the $S_1(2^1A_g^-)$/ICT excited state of 3′-hECN are clearly longer in the OCP^o subpopulations (5.2 and 11 ps in OCP^o and 3.2 and 7.1 ps in OCP^r). The spectral shapes of the TA spectra in the NIR range show that the subpopulation with a shorter lifetime contains 3′-hECN with enhanced ICT character of the $S_1(2^1A_g^-)$/ICT state that is clearly demonstrated by an elevated amplitude of SE.

Is Adjustment of the S_1 State Energy of 3′-hECN Important for Photoprotective Properties of OCP? The TA results we have collected in the NIR spectral range allowed us to estimate the energy of the $S_1(2^1A_g^-)$/ICT state of 3′-hECN bound in both OCP forms and check the correctness of earlier efforts. The energies that we have obtained differ considerably from those obtained previously. This is simply due to the fact that previous attempts were based on presuppositions that later turned out to be not quite correct—it was assumed that OCP^o and OCP^r are clearly distinguished by fast and slow decay of $S_1(2^1A_g^-)$/ICT state of 3′-hECN.[11]

Nevertheless, our findings support suggestions drawn previously that both the OCP^o and OCP^r are energetically suitable for efficient quenching of PBS.[9] Most recent mass spectrometric studies of chemically cross-linked OCP^r and PBS, demonstrated that the OCP^r interacts with APC_{660} and ACP_{680} allophycocyanin trimers in the PBS core,[12] confirming previous findings from time-resolved fluorescence spectroscopy of in vivo and isolated PBS−OCHP complexes.[32,33] Therefore, the OCP^r presumably quenches fluorescence from both APC_{660} and ACP_{680} emitting light at 660 and 680 nm. These wavelengths correspond to 15,150 and 14,700 cm^{-1}, respectively, energies that are considerably higher than the $S_1(2^1A_g^-)$/ICT energy of 3′-hECN in either inactive (13,750 cm^{-1}) or active (12,300 cm^{-1}) OCP (long-lived subpopulations). Note that dominant, short-lived subpopulations of both OCPs will have even lower energies of the $S_1(2^1A_g^-)$/ICT state.

Our recent studies on the dynamics of OCP^o-to-OCP^r conversion with application of native electrospray ionization mass spectroscopy demonstrated that the photoactivation process is associated with monomerization of the protein that in the inactive form is mostly dimerized.[12] Therefore, it seems that an aggregation stage of the protein, not modification of excited state properties of the bound carotenoid molecule, is more crucial for quenching properties of the OCP. Consequently, we support the view proposed by Polivka and coworkers in their recent work,[9] that the downshift of the $S_1(2^1A_g^-)$/ICT state of 3′-hECN, observed during the OCP^o-to-OCP^r transformation, is only a side effect of the protein structural changes but it does not improve OCP quenching properties.

AUTHOR INFORMATION

Corresponding Author

*Telephone: +1 314 935-7971; fax +1 314 935-4432; e-mail: blankenship@wustl.edu.

Notes

The authors declare no competing financial interest.

ACKNOWLEDGMENTS

This research was performed as a part of the Photosynthetic Antenna Research Center, an Energy Frontier Research Center

funded by the U.S. DOE, Office of Basic Energy Sciences (Grant No. DE-SC 0001035 to R.E.B).

REFERENCES

(1) Wilson, A.; Punginelli, C.; Gall, A.; Bonetti, C.; Alexandre, M.; Routaboul, J. M.; Kerfeld, C. A.; van Grondelle, R.; Robert, B.; Kennis, J. T. M.; et al. A Photoactive Carotenoid Protein Acting as Light Intensity Sensor. *Proc. Natl. Acad. Sci. U.S.A.* **2008**, *105*, 12075−12080.

(2) Wilson, A.; Kinney, J. N.; Zwart, P. H.; Punginelli, C.; D'Haene, S.; Perreau, F.; Klein, M. G.; Kirilovsky, D.; Kerfeld, C. A. Structural Determinants Underlying Photoprotection in the Photoactive Orange Carotenoid Protein of Cyanobacteria. *J. Biol. Chem.* **2010**, *285*, 18364−18375.

(3) Kirilovsky, D.; Kerfeld, C. A. The Orange Carotenoid Protein: A Blue-Green Light Photoactive Protein. *Photochem. Photobiol. Sci.* **2013**, *12*, 1135−1143.

(4) Kirilovsky, D.; Kerfeld, C. A. The Orange Carotenoid Protein in Photoprotection of Photosystem II in Cyanobacteria. *Biochim. Biophys. Acta-Bioenergetics* **2012**, *1817*, 158−166.

(5) Kirilovsky, D. Photoprotection in Cyanobacteria: The Orange Carotenoid Protein (OCP)-Related Non-photochemical-Quenching Mechanism. *Photosynth. Res.* **2007**, *93*, 7−16.

(6) Bailey, S.; Grossman, A. Photoprotection in Cyanobacteria: Regulation of Light Harvesting. *Photochem. Photobiol.* **2008**, *84*, 1410−1420.

(7) Leverenz, R. L.; Jallet, D.; Li, M. D.; Mathies, R. A.; Kirilovsky, D.; Kerfeld, C. A. Structural and Functional Modularity of the Orange Carotenoid Protein: Distinct Roles for the N- and C-Terminal Domains in Cyanobacterial Photoprotection. *Plant Cell* **2014**, *26*, 426−437.

(8) Kerfeld, C. A.; Sawaya, M. R.; Brahmandam, V.; Cascio, D.; Ho, K. K.; Trevithick-Sutton, C. C.; Krogmann, D. W.; Yeates, T. O. The Crystal Structure of a Cyanobacterial Water-Soluble Carotenoid Binding Protein. *Structure* **2003**, *11*, 55−65.

(9) Polivka, T.; Chabera, P.; Kerfeld, C. A. Carotenoid-Protein Interaction Alters the S-1 Energy of Hydroxyechinenone in the Orange Carotenoid Protein. *Biochim. Biophys. Acta-Bioenergetics* **2013**, *1827*, 248−254.

(10) Berera, R.; Gwizdala, M.; van Stokkum, I. H.; Kirilovsky, D.; van Grondelle, R. Excited States of the Inactive and Active Forms of the Orange Carotenoid Protein. *J. Phys. Chem. B* **2013**, *117*, 9121−9128.

(11) Polivka, T.; Kerfeld, C. A.; Pascher, T.; Sundstrom, V. Spectroscopic Properties of the Carotenoid 3′-Hydroxyechinenone in the Orange Carotenoid Protein from the Cyanobacterium *Arthrospira maxima*. *Biochemistry* **2005**, *44*, 3994−4003.

(12) Zhang, H.; Liu, H. J.; Niedzwiedzki, D. M.; Prado, M.; Jiang, J.; Gross, M. L.; Blankenship, R. E. Molecular Mechanism of Photoactivation and Structural Location of the Cyanobacterial Orange Carotenoid Protein. *Biochemistry* **2014**, *53*, 13−19.

(13) Berera, R.; van Stokkum, I. H. M.; Gwizdala, M.; Wilson, A.; Kirilovsky, D.; van Grondelle, R. The Photophysics of the Orange Carotenoid Protein, a Light-Powered Molecular Switch. *J. Phys. Chem. B* **2012**, *116*, 2568−2574.

(14) Niedzwiedzki, D. M.; Fuciman, M.; Frank, H. A.; Blankenship, R. E. Energy Transfer in an Lh4-Like Light Harvesting Complex from the Aerobic Purple Photosynthetic Bacterium *Roseobacter denitrificans*. *Biochim. Biophys. Acta-Bioenergetics* **2011**, *1807*, 518−528.

(15) Polivka, T.; Sundstrom, V. Ultrafast Dynamics of Carotenoid Excited States-from Solution to Natural and Artificial Systems. *Chem. Rev.* **2004**, *104*, 2021−2071.

(16) Polivka, T.; Sundstrom, V. Dark Excited States of Carotenoids: Consensus and Controversy. *Chem. Phys. Lett.* **2009**, *477*, 1−11.

(17) Mendes-Pinto, M. M.; Sansiaume, E.; Hashimoto, H.; Pascal, A. A.; Gall, A.; Robert, B. Electronic Absorption and Ground State Structure of Carotenoid Molecules. *J. Phys. Chem. B* **2013**, *117*, 11015−11021.

(18) Mendes-Pinto, M. M.; Galzerano, D.; Telfer, A.; Pascal, A. A.; Robert, B.; Ilioaia, C. Mechanisms Underlying Carotenoid Absorption in Oxygenic Photosynthetic Proteins. *J. Biol. Chem.* **2013**, *288*, 18758−18765.

(19) Ehlers, F.; Wild, D. A.; Lenzer, T.; Oum, K. Investigation of the S_1/Ict→S_0 Internal Conversion Lifetime of 4′-Apo-β-caroten-4′-al and 8′-apo-β-caroten-8′-al: Dependence on Conjugation Length and Solvent Polarity. *J. Phys. Chem. A* **2007**, *111*, 2257−2265.

(20) van Stokkum, I. H.; Larsen, D. S.; van Grondelle, R. Global and Target Analysis of Time-Resolved Spectra. *Biochim. Biophys. Acta-Bioenergetics* **2004**, *1657*, 82−104.

(21) Frank, H. A.; Bautista, J. A.; Josue, J.; Pendon, Z.; Hiller, R. G.; Sharples, F. P.; Gosztola, D.; Wasielewski, M. R. Effect of the Solvent Environment on the Spectroscopic Properties and Dynamics of the Lowest Excited States of Carotenoids. *J. Phys. Chem. B* **2000**, *104*, 4569−4577.

(22) Zigmantas, D.; Hiller, R. G.; Sharples, F. P.; Frank, H. A.; Sundstrom, V.; Polivka, T. Effect of a Conjugated Carbonyl Group on the Photophysical Properties of Carotenoids. *Phys. Chem. Chem. Phys.* **2004**, *6*, 3009−3016.

(23) Zigmantas, D.; Polivka, T.; Hiller, R. G.; Yartsev, A.; Sundstrom, V. Spectroscopic and Dynamic Properties of the Peridinin Lowest Singlet Excited States. *J. Phys. Chem. A* **2001**, *105*, 10296−10306.

(24) Bautista, J. A.; Connors, R. E.; Raju, B. B.; Hiller, R. G.; Sharples, F. P.; Gosztola, D.; Wasielewski, M. R.; Frank, H. A. Excited State Properties of Peridinin: Observation of a Solvent Dependence of the Lowest Excited Singlet State Lifetime and Spectral Behavior Unique among Carotenoids. *J. Phys. Chem. B* **1999**, *103*, 8751−8758.

(25) Stalke, S.; Wild, D. A.; Lenzer, T.; Kopczynski, M.; Lohse, P. W.; Oum, K. Solvent-Dependent Ultrafast Internal Conversion Dynamics of *n*′-Apo-beta-carotenoic-*n*′-acids (*n* = 8, 10, 12). *Phys. Chem. Chem. Phys.* **2008**, *10*, 2180−2188.

(26) Chatterjee, N.; Niedzwiedzki, D. M.; Kajikawa, T.; Hasegawa, S.; Katsumura, S.; Frank, H. A. Effect of π-Electron Conjugation Length on the Solvent-Dependent S_1 Lifetime of Peridinin. *Chem. Phys. Lett.* **2008**, *463*, 219−224.

(27) Chatterjee, N.; Niedzwiedzki, D. M.; Aoki, K.; Kajikawa, T.; Katsumura, S.; Hashimoto, H.; Frank, H. A. Effect of Structural Modifications on the Spectroscopic Properties and Dynamics of the Excited States of Peridinin. *Arch. Biochem. Biophys.* **2009**, *483*, 146−155.

(28) Niedzwiedzki, D. M.; Chatterjee, N.; Enriquez, M. M.; Kajikawa, T.; Hasegawa, S.; Katsumura, S.; Frank, H. A. Spectroscopic Investigation of Peridinin Analogues Having Different π-Electron Conjugated Chain Lengths: Exploring the Nature of the Intramolecular Charge Transfer State. *J. Phys. Chem. B* **2009**, *113*, 13604−13612.

(29) Niedzwiedzki, D. M.; Kajikawa, K.; Aoki, K.; Katsumura, S.; Frank, H. Excited States Energies and Dynamics of Peridinin Analogues and the Nature of the Intramolecular Charge Transfer State in Carbonyl-Containing Carotenoids. *J. Phys. Chem. B* **2013**, *117*, 6874−6887.

(30) Chabera, P.; Fuciman, M.; Hribek, P.; Polivka, T. Effect of Carotenoid Structure on Excited-State Dynamics of Carbonyl Carotenoids. *Phys. Chem. Chem. Phys.* **2009**, *11*, 8795−8803.

(31) Polivka, T.; Kaligotla, S.; Chabera, P.; Frank, H. A. An Intramolecular Charge Transfer State of Carbonyl Carotenoids: Implications for Excited State Dynamics of Apo-carotenals and Retinal. *Phys. Chem. Chem. Phys.* **2011**, *13*, 10787−10796.

(32) Tian, L. J.; Gwizdala, M.; van Stokkum, I. H. M.; Koehorst, R. B. M.; Kirilovsky, D.; van Amerongen, H. Picosecond Kinetics of Light Harvesting and Photoprotective Quenching in Wild-Type and Mutant Phycobilisomes Isolated from the Cyanobacterium *Synechocystis* PCC 6803. *Biophys. J.* **2012**, *102*, 1692−1700.

(33) Tian, L. J.; van Stokkum, I. H. M.; Koehorst, R. B. M.; Jongerius, A.; Kirilovsky, D.; van Amerongen, H. Site, Rate, and Mechanism of Photoprotective Quenching in Cyanobacteria. *J. Am. Chem. Soc.* **2011**, *133*, 18304−18311.